PCCP

ROYAL SOCIETY OF CHEMISTRY

PAPER

View Article Online
View Journal | View Issue

Cite this: *Phys. Chem. Chem. Phys.*, 2025, **27**, 17572

H-bonding-assisted energy retention in bicyclic diene photoswitches for rechargeable solar thermal batteries: CASSCF, CASPT2, and DLPNO-CCSD(T) insights

Akanksha Ashok Sangolkar, Rama Krishna Kadiyam, Sibam Sahu and Ravinder Pawar *

Molecular solar thermal (MOST) systems have the potential to harness and store a vast amount of solar energy, making them promising for renewable energy solutions. However, the integration of solar absorption, high energy storage density, and long thermal half-life into a single photochromic couple remains a contemporary challenge, hindering their practical deployment. In this work, we present a rational design strategy to enhance key properties of a bridged bicyclic diene (BBD)-based photoswitch through elongation of the unsaturated bridge and strategic functionalization. The introduced substituents promote synergistic non-covalent interactions, particularly intramolecular hydrogen bonding and reinforce push–pull electronic effects, collectively enabling pronounced bathochromic shifts in absorption without compromising energy storage capacity and duration. Comprehensive electronic structure analyses carried out using the CASSCF, CASPT2, and DLPNO-CCSD(T) methods ensure the robustness of the findings. This study provides valuable design principles for next-generation MOST systems by leveraging the cooperative effects of non-covalent interactions and electronic modulation through functionalization.

Received 21st April 2025,
Accepted 22nd July 2025

DOI: 10.1039/d5cp01525a

rsc.li/pccp

1. Introduction

Energy is an inevitable necessity whose demand is growing continuously with the growth of global population, industrialization, and economic development.[1] The inadequacy of our primary energy resource, *i.e.* fossil fuels, and its associated environmental problems leading to catastrophic climate change necessitate the transition towards renewable and sustainable energy resources.[2–4] As the sun is the most powerful and fundamental energy resource for Earth, scientific advancements are underway for the development of artificial light-harvesting technologies such as photovoltaic cells, photocatalytic H_2 generation through H_2O splitting, and CO_2 reduction to methanol for its direct utilization.[5–11]

A molecular solar thermal (MOST) system is a carbon-neutral energy storage technology that was previously overlooked by the scientific community but is recently gaining prominence.[12,13] The standout characteristic of MOST systems is their ability to harness solar energy, store it as chemical energy for sufficiently long durations, and release thermal energy as an output, providing an innovative storage solution for intermittent solar radiation.[12,13] The process operates in a closed, emission-free cycle where a solar thermal battery gets charged with the capture of photons and discharges with the release of thermal energy, exchanging heat with the surroundings without exchanging matter.[14]

Photoswitches are light-responsive molecules that undergo isomerization to form a metastable photoproduct upon illumination and can be reverted to the parent isomer when triggered by an external stimulus and are the vital functional units of MOST devices.[15–19] Bridged bicyclic diene (BBD)-based norbornadiene (NBD)/quadricyclane (QC) has been recognized as a promising photoswitching couple for MOST systems owing to its high gravimetric energy density and energy storage time.[12,13,20] However, the strong optical absorption of NBD in the UV region and its spectral overlap with QC impose hurdles for its real-world applications.[12,13,20] Strategic incorporation of electron-donating and electron-withdrawing groups offers a viable route to tune the electronic structure. Consequently, research has been conducted exploring multiple design approaches, such as implementing push–pull effects, introducing steric hindrance, and constructing donor–acceptor dimers and oligomers to tailor their light absorption characteristics.[20–22] However, designing photochromic systems has historically faced significant challenges as red-shifting in the absorption properties

Laboratory of Advanced Computation and Theory for Materials and Chemistry, Department of Chemistry, National Institute of Technology Warangal (NITW), Warangal, Telangana- 506004, India. E-mail: ravinder_pawar@nitw.ac.in

either compromises energy density or energy retention time.[12,13,20] This inherent trade-off has made it difficult to integrate all essential features, posing a contemporary challenge and necessitating the rational engineering of the photoswitches. Boulatov and co-workers emphasized that the major bottleneck behind the lack of a practical MOST system does not lie in the concept of photoswitching but in the failure of an optimal molecular design; conventional chemistry ideas will essentially assist in tackling the challenge.[14,23]

Moth-Poulsen and co-workers have devoted continuous efforts to improve molecular designs, which have significantly enhanced the properties of photoswitching systems to achieve practical solutions.[21,24–30] Recent advancements toward the development of a single photoswitch integrating all essential features for practical applications have been systematically reviewed.[31–37] Despite several advancements, there are numerous prospects to tailor the properties of photoswitches, making them suitable for high energy density solar thermal systems as next-generation rechargeable fuels.

Moth-Poulsen, Mikkelsen and colleagues demonstrated that the energy storage performance of a bicyclooctadiene/tetracyclooctane (BOD/TCO) couple with an elongated saturated bridge exceeds that of the structurally analogous NBD/QC (Fig. 1).[38–40] Inspired by these findings, subsequent research efforts have focused on investigating photoswitches with structurally modified BOD skeletons to further optimize their properties.[41–45] The progressive elongation of the saturated bridge enhances the energy storage capacity, albeit at the cost of reduced storage lifetimes due to increased ring strain energy (RSE) in the photoproduct.[44,46] Structure–RSE–property correlations revealed that elongation of an unsaturated bridge can concurrently improve both the energy storage density and thermal half-lives, thereby offering promising properties in a single candidate.[41,45] This improvement is achieved due to a reduced strain in both photoisomers while maintaining a large enthalpy difference between them.[41,45] Owing to their structural similarity, the photoswitching mechanism of these systems resembles that of the NBD/QC pair and other related BBD-based systems.[45] In analogy with the NBD/QC system, these photochromic couples absorb strongly in the core UV region due to a lack of conjugation and substitution may diminish their energy storage performance.[41,45,46]

The non-covalent interactions, such as T-shaped interactions, in arylazopyrazoles can effectively stabilize the *Z*-isomer, thereby prolonging the thermal half-life.[47,48] Yet, to the best of our knowledge, no studies have synergistically leveraged both non-covalent interaction design and electronic functionalization to integrate all desired features within BBD-based photoswitches.

This study aims to induce a bathochromic shift in the absorption profile of photoswitches without compromising their thermochemical performance, thereby improving their viability for real-world MOST applications. To this end, six BBD-based photoswitches with elongated unsaturated bridges were designed to facilitate push–pull effects through strategic functionalization. Comprehensive quantum chemical calculations were conducted using density functional theory (DFT)-based M06-2X and PBE functionals and *ab initio* methods, including DLPNO-CCSD(T), CASSCF, and CASPT2, to ensure reliable energetic and electronic characterization. Solvation effects on the properties of the photoswitches have also been elucidated to identify optimal conditions for their practical integration into MOST devices. The results underscore the synergistic influence of non-covalent interactions and donor–acceptor substitution in modulating absorption into the desired spectral range while concurrently achieving high energy storage density and extended thermal half-lives within a single photoswitch.

2. Computational methodology

The geometries of the parent isomers and photoproducts were fully relaxed by means of the DFT-based M06-2X functional in conjunction with the 6-311++G** Pople-style basis set.[49]

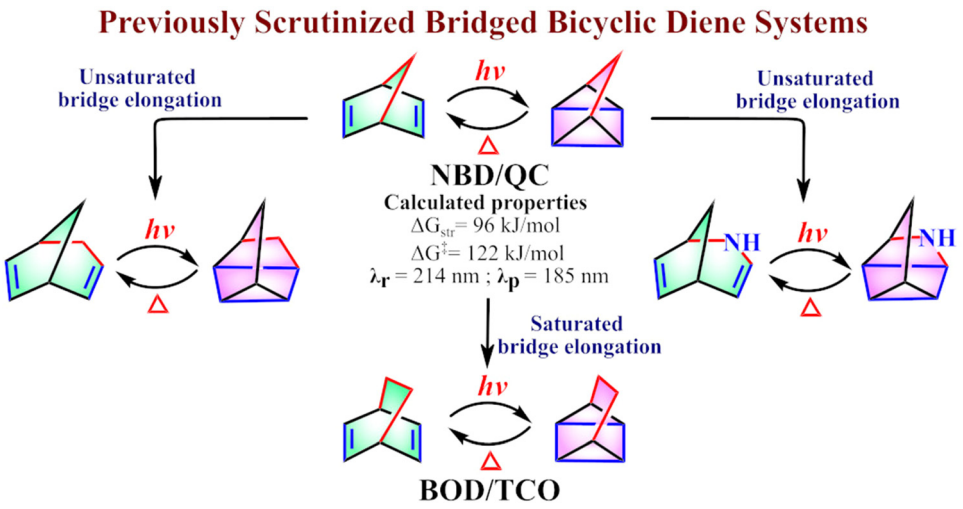

Fig. 1 Overview of previously investigated bridged bicyclic diene (BBD) photoswitches.

This method was chosen because previous benchmarking studies have shown that the M06-2X functional performs well in accurately predicting the structure and photoswitching properties of NBD/QC and BOD/TCO couples at low computational cost.[39,50] Analytical second-order derivatives were computed at the same level of theory to analyse the nature of the critical point structures using harmonic frequency calculations. The stationary point structure was confirmed as a local minimum on the potential energy surface (PES) by verifying the absence of an imaginary frequency. These optimized geometries were subsequently used for all further calculations carried out in this study. The first 15 singlet vertical electronic excited states were computed at the time-dependent TD-M06-2X/6-311++G** level of theory to scrutinize the absorption properties of the photoisomers.

The storage energy (ΔG_{str}) of a photoswitching couple represents the amount of solar energy harvested and stored in the metastable isomer, which can subsequently be released as heat upon thermal or photochemical activation. It is computed as the difference in Gibbs free energy between the photogenerated isomer and the original diene structure:

$$\Delta G_{str} = G_{photoproduct} - G_{diene} \quad (1)$$

where G_{diene} and $G_{photoproduct}$ represent the Gibbs free energies of the parent and metastable isomers, respectively. To ensure accurate estimation of energy storage capacities, single-point energies were computed at the DLPNO-CCSD(T)/Def2-TZVP level of theory.[51] The storage energy $\Delta G_{str}^{DLPNO\text{-}CCSD(T)}$ was computed by combining the electronic energy difference between the two photoisomers refined at DLPNO-CCSD(T)/Def2-TZVP and thermal corrections derived from M06-2X/6-311++G** calculations, analogous to previous reports.[17,46,52,53]

$$\Delta G_{str}^{DLPNO\text{-}CCSD(T)} = \Delta E_{str}^{DLPNO\text{-}CCSD(T)} + \Delta T_{str}^{M06\text{-}2X} \quad (2)$$

where $\Delta E_{str}^{DLPNO\text{-}CCSD(T)}$ denotes the electronic energy difference at the DLPNO-CCSD(T) level, and $\Delta T_{str}^{M06\text{-}2X}$ corresponds to the thermal correction difference between the two photoisomers at the M06-2X level.

The conversion of the metastable photoproduct back to the parent diene in the absence of light is termed thermal back reaction (TBR) or thermal back isomerization. The activation energy associated with this process is referred to as the TBR barrier. Since the ring opening of the [2+2]-cycloadduct is thermally forbidden according to the Woodward–Hoffmann rules, the back reversion proceeds through an asynchronous yet concerted mechanism at elevated temperatures involving the formation of biradicals.[21,54–56]

Single-reference methods are inappropriate, while multi-reference methods are more suitable for describing biradicals. The multiconfigurational complete active space with the second-order perturbation theory (CASPT2) method is computationally demanding, and its vibrational frequency calculations can be inaccurate due to reliance on numerical differentiation.[57] As a result, the less expensive multiconfigurational complete active space self-consistent field (CASSCF) method can be preferred for locating the geometries of transition states (TS).[58] An active space consisting of four occupied (four σ) and four virtual (four σ*) orbitals in the photoproduct was adequate to model the photoswitching mechanism in the NBD/QC couple.[46] This follows the precedent set by Kuisma *et al.*, who demonstrated that (8,8)-CASSCF offers a good compromise between computational efficiency and accuracy.[55] Therefore, the TS structures were initially optimized using the (8,8)-CASSCF/6-311++G** method. The active space was extended to include a nitrogen lone pair (lp_N), resulting in a (10,9)-CASSCF/6-311++G** treatment for nitrogen-containing systems where the effects of conjugated lone pairs are significant.

Despite being a single-reference method, previous benchmarking studies have shown that the PBE functional reliably predicts the geometries of the NBD/QC couple, owing to its better alignment of donor and acceptor groups.[55] Consequently, TSs involved during TBR in BBD-based systems were earlier located using the climbing-image nudged elastic band (CI-NEB) method with the PBE functional.[46,55] In this study, the geometries of the TSs were similarly optimized using the PBE functional in combination with the 6-311++G** basis set using Gaussian16, analogous to our recent reports.[41,45,59] The TS structures were characterized as first-order saddle points on the PES as they exhibited a single imaginary frequency with displacement vectors in the direction of bond formation and breaking.

The PBE functional tends to overestimate TS energies due to its inadequate treatment of multiconfigurational behaviour. Likewise, the CASSCF method neglects dynamic electron correlation, which results in an exaggeration of the TS energies. Although both methods are more suitable for obtaining TS geometries, the inherent limitations make them less reliable for accurately predicting energetics.[55] An accurate estimation of the TBR barrier thus requires a method that accounts for both multiconfigurational behavior and electron correlation. Consequently, prior studies have employed geometry optimizations at the PBE level, followed by single-point energy evaluations using the CASPT2 method.[17,52,55,57] In line with this protocol, we performed single-point energy calculations at the CASPT2 level using the 6-311++G** basis set on geometries optimized using both the PBE and CASSCF methods.[57] The photoswitching systems whose unsaturated bridge was elongated with a methylene (–CH_2–) unit were modelled using (8,8)-CASPT2, while those elongated with imine (–NH–) were modeled with (10,9)-CASPT2 to consider the presence of lp_N on conjugated nitrogen. The TBR barrier $\left(\Delta E_{TBR}^{\ddagger}\right)$ was calculated as:

$$\Delta E_{TBR}^{\ddagger} = E_{TS} - E_{photo\ product} \quad (3)$$

To assess the influence of solvation, the geometries of the photoisomers were fully optimized at the M06-2X/6-311++G** level, while those of the TSs were optimized at the PBE/6-311++G** level, both in the presence of solvents. Cyclohexane (ε = 2.02), dichloromethane (ε = 8.93), and acetonitrile (ε = 35.69) were employed to examine the effect of solvent polarity (dielectric constant). Harmonic frequency calculations were performed at the same level to confirm the nature of each

stationary point as a local minimum or a first-order saddle point. Subsequent single-point energy calculations were carried out at the DLPNO-CCSD(T)/Def2-TZVP or CASPT2/6-311++G** level of theory to accurately evaluate thermochemical properties. Additionally, the first 15 singlet vertical excitation energies were computed using TD-M06-2X/6-311++G** in the presence of solvents to investigate the absorption characteristics. Throughout all geometry optimizations and single-point calculations, solvent effects were modelled implicitly using the continuum solvation model density (SMD) model.

DFT and TD-DFT calculations were performed using Gaussian16, while the single-point calculations at the DLPNO-CCSD(T) and CASPT2/6-311++G** levels were carried out employing the ORCA package.[60,61] Non-covalent interactions between the different substituents in photoisomers at two thermodynamic states were examined using the interaction region indicator (IRI) utilizing the Multiwfn program.[62,63]

3. Results and discussion

Unsubstituted BBD-based systems featuring elongated unsaturated bridges have previously been shown to undergo photoisomerization *via* a mechanism analogous to that of the NBD/QC pair.[45] In the present study, BBD systems with elongated unsaturated bridges were selected due to their demonstrated thermochemical advantages, namely high energy storage densities and prolonged thermal half-lives (τ), which render them promising candidates for practical MOST applications.[41,45] However, these unsubstituted systems absorb predominantly in the UV region, limiting their efficiency under solar irradiation.[41,45] To address this shortcoming, a series of six rationally functionalized BBD photoswitches (**Sub$_1$** to **Sub$_6$**), illustrated in Scheme 1, were designed and evaluated to achieve red-shifted absorption profiles while preserving MOST-relevant thermochemical properties.

In the **Sub$_1$** system, an electron-donating methoxyphenyl (MeO–Ph–) group and an electron-withdrawing cyano (–CN) group were placed on the non-elongated unsaturated bridge. In **Sub$_2$**, the same substituents were relocated to the elongated unsaturated bridge. **Sub$_3$** differs from **Sub$_1$** by incorporating an electron-donating methyl aniline (MeNH–Ph–) group in place of the MeO–Ph– group, thereby altering the donor strength and conjugation characteristics.

It is well established that the incorporation of electron-donating and electron-withdrawing substituents often compromises the thermochemical performance, and alternative strategies are required to circumvent this trade-off. To address the typical decline in energy storage capacity and duration induced by substitution, we explored an approach that integrates H-bonding interactions with the push–pull electronic effect through strategic functionalization. In the **Sub$_4$** system, an additional hydroxyl (–OH) group is introduced at the elongated unsaturated bridge relative to **Sub$_3$**, with the intent to facilitate intramolecular H-bonding with substituents located on the adjacent non-elongated unsaturated bridge. In both **Sub$_5$** and **Sub$_6$**, the unsaturated bridge is elongated with an –NH– linker, and the methoxyphenyl (MeO–Ph–) and cyano (–CN) groups are positioned on the non-elongated and elongated bridges, respectively. This dual strategy aims to balance electronic tuning and structural stabilization, mitigating the thermochemical penalties typically associated with strong substituent effects.

The photoswitching process operates *via* a sequential mechanism comprising the photoinduced conversion of the parent diene into a metastable photoproduct ([2+2]-cycloadduct) and its subsequent reversion to the original diene (Scheme 1).[18,45] Upon light absorption, the parent diene undergoes a vertical

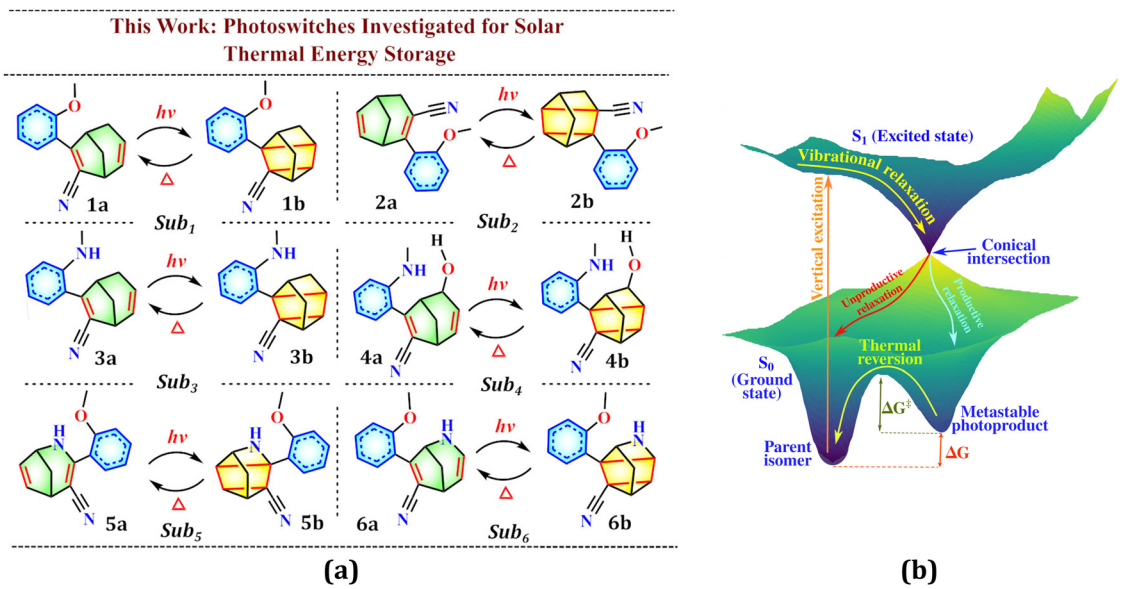

Scheme 1 (a) Functionalized BBD-based photoswitches with extended unsaturated bridges evaluated for MOST applications and (b) the potential energy landscape illustrating the photoswitching process.

electronic transition to the Franck–Condon region of the excited state. Subsequently, structural reorganization is initiated as the system evolves toward the minimum on the excited-state PES. Vibrational relaxation drives the molecule to a conical intersection (CI), a region where the excited-state and ground-state PESs intersect, enabling non-radiative decay to the ground state (S_0).[18,45] This process results in the formation of a metastable [2+2]-photoproduct, which is a high-energy species residing at a local minimum of the S_0 state. Depending on its thermal stability, this metastable isomer may spontaneously revert to the parent diene or require an external stimulus such as heat, light, or a catalyst to trigger back-isomerization. For real-world MOST applications, thermo-reversible photoswitches are particularly attractive, as they enable long-term energy storage in the form of the metastable isomer. Upon demand, the stored energy can be released through controlled thermal activation, allowing for efficient energy release.

3.1 Thermochemical properties

Energy storage capacity and duration are crucial metrics for evaluating the suitability of photoswitching couples for solar thermal energy storage. To identify promising candidates, the work commenced with the assessment of thermochemical parameters, including energy storage capacity and thermal stability of the metastable isomer. The optimized ground-state geometries of the functionalized dienes, their corresponding metastable photoproducts (M06-2X/6-311++G**) and TS geometries (PBE/6-311++G**) are shown in Fig. S1 (S I of SI). Additionally, Cartesian coordinates for all optimized geometries are available in a consolidated file, Cartesian.xyz, included in the SI.

3.1.1. Energy storage capacity. The energy storage capacities of functionalized switches calculated using M06-2X/6-311++G** and DLPNO-CCSD(T)/Def2-TZVP methods are depicted by histograms in Fig. 2, with numerical values listed in Table S1 (S II of SI). The DLPNO-CCSD(T) calculations indicate that the storage energy for all systems falls in the range of 133.6 to 167.7 kJ mol^{-1}, demonstrating their strong potential for energy storage applications. The functionalized systems **Sub_5** and **Sub_6**, where the unsaturated bridge is elongated *via* –NH– exhibit the highest storage energy of 167.7 and 163.3 kJ mol^{-1}, respectively. Likewise, the **Sub_4** system, featuring an extended unsaturated bridge with $–CH_2–$ unit, also has a high storage energy of 150.9 kJ mol^{-1}. Interestingly, these energy values surpass that of the pristine NBD/QC couple (96 kJ mol^{-1}) and exceed those of other photoswitches of the MOST quartet.[12] This enhancement is primarily attributed to the elongation of the unsaturated bridge, which stabilizes both photoisomers by alleviating ring strain while preserving a large enthalpy difference between them, as elaborated in our previous study.[45] The M06-2X functional underestimates energy values (121.1–162.2 kJ mol^{-1}) compared to DLPNO-CCSD(T); nevertheless, both computational methods yield the same overall trend.

Indeed, the gravimetric energy storage density (ESD) is a better entity for describing energy storage capacity than the absolute storage energy. The estimated ESD values for the studied functionalized systems are illustrated in the bar graph shown in Fig. 2. Notably, the ESD for all functionalized systems (563.5–704.2 kJ kg^{-1}) exceeds the benchmark value of 300 kJ kg^{-1}, which is considered the minimum ideal threshold for MOST systems.[13] Therefore, all the functionalized BBD-based systems show strong potential for harvesting and storing large amounts of solar energy, as required for MOST applications. Akin to the storage energy, **Sub_4**, **Sub_5**, and **Sub_6** (598.6, 704.2, and 685.7 kJ kg^{-1}) stand out as the most energy-dense solar thermal fuels amidst the studied functionalized systems. As the considered substituents have roughly similar masses, the ESD values follow the same trend as that of storage energy.

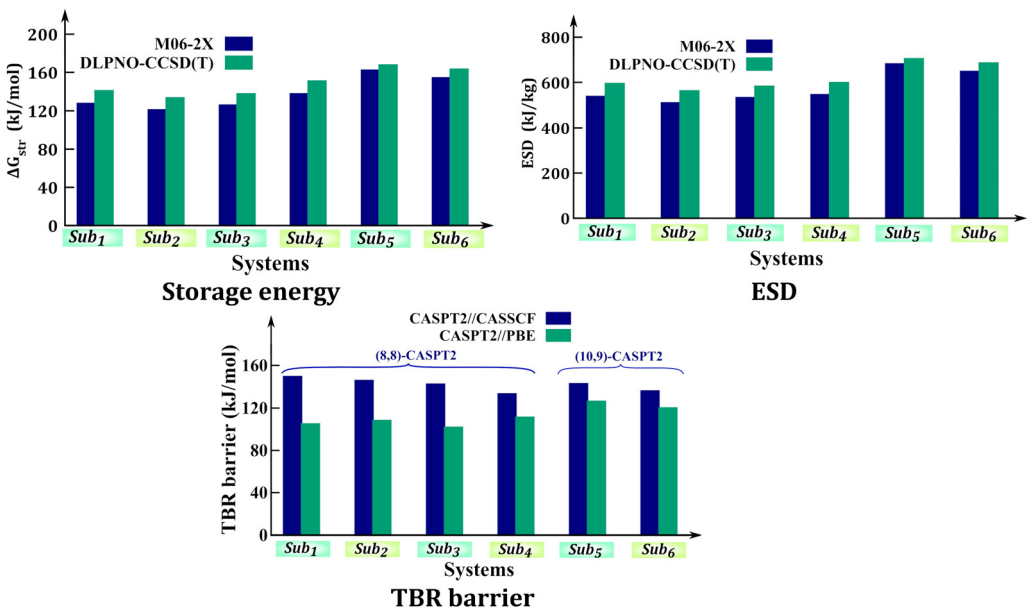

Fig. 2 Thermochemical properties of the functionalized BBD-based systems featuring an elongated unsaturated bridge calculated using different computational methods.

3.1.2. Energy storage duration. Subsequent analysis focused on obtaining precise TBR barriers $\left(\Delta E^{\ddagger}_{\mathrm{TBR}}\right)$, with refined electronic energies at the CASPT2/6-311++G** level for the TS geometries obtained with CASSCF and PBE methods in combination with the 6-311++G** basis set. The TBR barrier of the photoswitching system should be sufficiently high to prevent the spontaneous and rapid reversal of the photoproduct into the parent isomer, enabling the long-term storage of harnessed solar energy for real-world applications. The TBR barriers were computed using the (8,8)-CASPT2 method for functionalized systems **Sub$_1$** to **Sub$_4$**, where the unsaturated bridge is extended with a –CH_2– unit. For **Sub$_5$** and **Sub$_6$** systems, whose bridge is elongated with an –NH– unit, the (10,9)-CASPT2 method was employed to account for the lp on N. The TBR barriers derived at both CASPT2//CASSCF and CASPT2//PBE levels in conjunction with 6-311++G** basis set are depicted in Fig. 2. The numerical data of TBR barrier, rate constant for thermal reversion and half-lives (τ) of metastable photoproducts are provided in Table S2 (S II of SI).

Despite functionalization, all these photochromic couples have high activation barriers for thermal reversion, ranging from 101.9 to 126.4 kJ mol^{-1} at the CASPT2//PBE level. The elevated barrier primarily arises from the elongated unsaturated bridge of BBD, which stabilizes the photoproduct more than QC by facilitating the formation of two four-membered and one three-membered ring. **Sub$_1$**, **Sub$_2$**, and **Sub$_3$** have the lowest TBR barriers with values of 105.0, 108.2, and 101.9 kJ mol^{-1}, respectively. These values are considerably lower than the TBR barrier of 149.6 kJ mol^{-1} for the unsubstituted BBD system with an elongated unsaturated bridge.[41,45] This highlights the impact of functionalization in reducing the thermal stability of the photoproduct, and as a result, their energy retention periods are relatively short (0.03 to 0.40 days).

Interestingly, **Sub$_4$** exhibits a TBR barrier of 111.2 kJ mol^{-1}, which is larger relative to **Sub$_3$**, despite both having similar substituents. This increase can be attributed to the presence of an additional –OH group in **Sub$_4$**, which is absent in **Sub$_3$**. The calculated half-life of 1.34 days of the metastable photoisomer ensures that the system can retain the harvested solar energy for relatively longer durations, making it a promising candidate for day-night energy storage cycles and potential window coating applications. The functionalized systems **Sub$_5$** and **Sub$_6$** have higher TBR barriers of 126.4 and 120.2 kJ mol^{-1} and exhibit the half-life of 51.47 years and 50.09 days, respectively. These values suggest that the photoproducts are sufficiently stable and exhibit prolonged energy retention, highlighting their strong potential for durable solar energy storage applications. The TBR barriers calculated using the CASPT2//CASSCF in conjunction with 6-311++G** basis set range from 133.5 to 149.5 kJ mol^{-1}, implying that CASPT2//CASSCF overestimates the TBR barriers compared to CASPT2//PBE (Table S2).

3.2. Photophysical properties

The absorption spectra of the functionalized dienes and photoproducts are depicted in Fig. 3. The spectral data, including the molar absorption coefficient (ε), absorption onset (λ_{onset}) defined as $\log(\varepsilon) = 2$, the first important absorption wavelength of BBD (λ_{r}) and photoproduct (λ_{p}) whose oscillatory strength (f) surpasses 0.2, are provided in Table S3 (S III of SI). All functionalized dienes exhibit absorption of significantly longer wavelengths than the parent NBD/QC (214.42 nm) and BOD/TCO (197.48 nm) couples.[44–46] The bathochromic shift evident in Fig. 3 is attributed to the operation of a push–pull mechanism facilitated by extended conjugation due to functionalization.

Efficient molecular solar thermal energy storage requires that the parent isomer absorbs light beyond 340 nm, where solar irradiance is more intense at the Earth's surface.[14] The functionalized dienes exhibit λ_{onset} values ranging from 334.6 to 461.3 nm, with λ_{r} red-shifted to 274.7–355.8 nm compared to their unsubstituted counterparts, which predominantly absorb in the core UV region. The most pronounced red-shifts are observed for dienes of **Sub$_3$** (355.8 nm) and **Sub$_4$** (350.0 nm), highlighting their potential for solar energy capture. Interestingly, the dienes absorb at significantly longer wavelengths than their corresponding photoproducts. Further, the f and ε associated with the first important absorption of photoproducts are notably low relative to the corresponding diene, with the absorption confined primarily to the deep UV region (Table S3). This results in minimal spectral overlap between the two photoisomers in the longer wavelength domain. The observed optical gaps between the two photoisomers are 97, 82, and 86 nm for **Sub$_3$**, **Sub$_4$**, and **Sub$_6$**, respectively and λ_{onset} gap ranges from 53 to 154 nm. Such spectral separation suppresses the formation of a photostationary state during photoisomerization, thereby enhancing the overall photoswitching efficiency.

To shed light on the distinct absorption profiles of the functionalized dienes, we analyzed the molecular orbitals involved in their electronic transitions. Close inspection reveals that the key excitations in the dienes arise predominantly from transitions between the highest occupied molecular orbitals (HOMO) and the lowest unoccupied molecular orbitals (LUMO), as illustrated in Fig. 3c.

The diene of **Sub$_1$** exhibits a more red-shifted absorption than **Sub$_2$**, which may be attributed to the functionalization at the non-elongated unsaturated bridge. The diene of **Sub$_3$** (355.8 nm) and **Sub$_4$** (350.0 nm) absorbs at longer wavelengths compared to **Sub$_1$** and **Sub$_2$**. In **Sub$_1$** and **Sub$_2$**, the HOMO is mainly localized on the π-bonding framework of BBD and the phenyl moiety and electronic excitation facilitates charge transfer to the LUMO, which is distributed over the phenyl ring and the –CN group. However, the HOMO in **Sub$_3$** and **Sub$_4$** extends over the π-system of BBD, the phenyl ring, and the nitrogen lone pair of the methyl aniline group. Meanwhile, the LUMO is localized on the phenyl ring and –CN group, with negligible contribution from the nitrogen lone pair. The pronounced bathochromic shift observed in **Sub$_3$** and **Sub$_4$** is attributed to the incorporation of a strong electron-donating methyl aniline group, which enhances the intramolecular push–pull interaction.

In **Sub$_5$**, the lone pair on the oxygen atom of the methoxyphenyl group is involved in intramolecular H-bonding with the

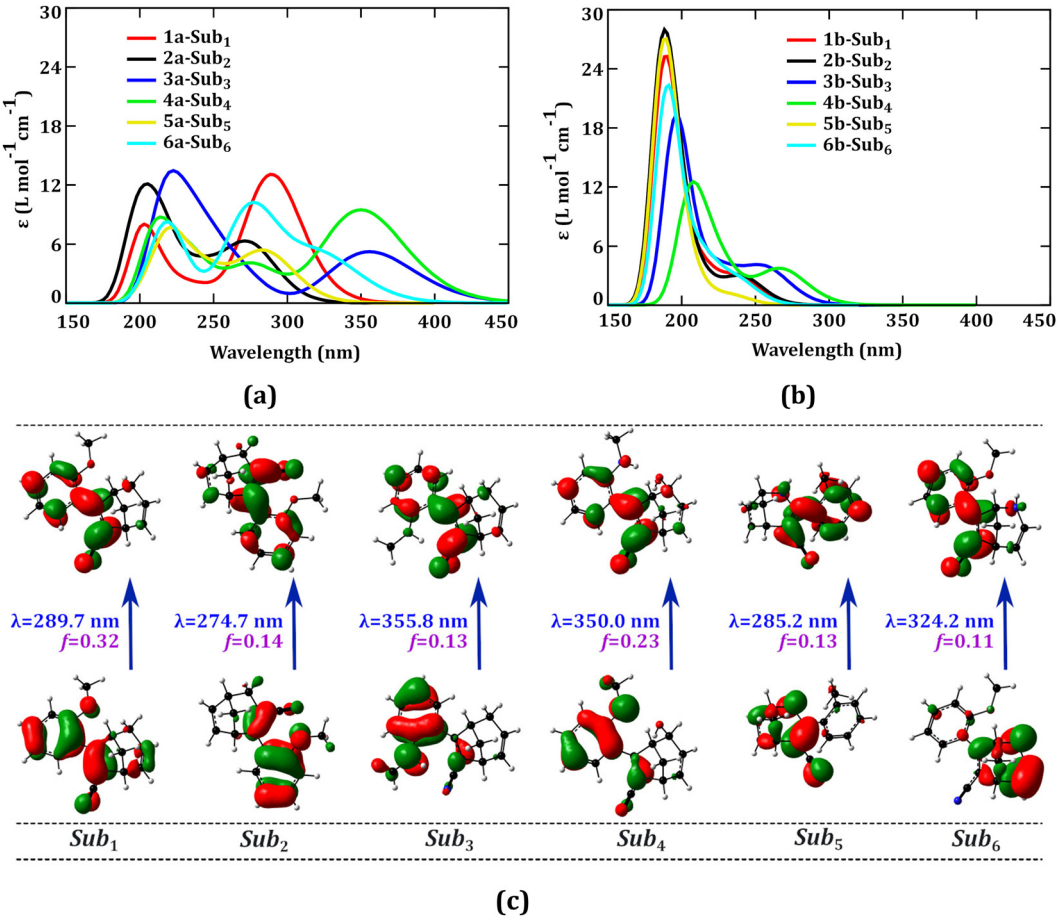

Fig. 3 Absorption properties of the functionalized BBD-based photoswitches (TD-M06-2X/6-311++G**). (a) Absorption profiles of dienes, (b) Absorption profiles of photoproducts, (c) Frontier molecular orbitals involved in the first important electronic excitation in dienes, highlighting the absorption wavelength and oscillatory strength.

–NH– group. This interaction reduces the electron-donating capacity of the methoxyphenyl group, effectively rendering the methoxyphenyl unit as electron-withdrawing. Consequently, the HOMO is localized on the π-framework of BBD, nitrogen lone pair, and –CN group, while the LUMO resides over the methoxyphenyl group. This weakens the push–pull effect; thus, **Sub$_5$** shows an absorption at 285.2 nm. These results underscore that the heteroatom responsible for push–pull enhancement should not engage in H-bonding interactions to ensure maximum bathochromic shift for efficient solar energy harnessing. In the case of **Sub$_6$**, the diene exhibits a pronounced bathochromic shift with the absorption wavelength at 324.2 nm. This shift arises from an electronic excitation from the HOMO, localized on the π-bonding orbital of BBD and the nitrogen lone pair to the LUMO, which is primarily distributed over the methoxyphenyl and –CN moieties.

3.3. Effect of solvation

Attention was focused on evaluating the influence of solvent polarity on the properties of functionalized BBD-based systems to optimize the conditions for MOST device integration. The variation in thermochemical properties of all solvated systems relative to the gas phase is illustrated in Fig. 4, with the corresponding numerical data presented in Table S4 (S IV of SI). The absorption profiles of the photoisomers of **Sub$_4$** in different polarity solvents are also presented in Fig. 4, while those for the other studied systems are provided in Fig. S2 (S IV of SI).

Solvent polarity exerts a significant influence on the thermochemical properties of the functionalized BBD-based systems. Generally, an increase in solvent polarity leads to a slight decrease in both storage energy and energy storage density, accompanied by a notable increase in the TBR barrier. However, **Sub$_2$** deviates from this trend, exhibiting an increase in both energy storage capacity (137.4 kJ mol^{-1}) and TBR barrier (116.0 kJ mol^{-1}) with increasing solvent polarity, indicating its enhanced suitability for MOST applications in polar solvents. In acetonitrile, **Sub$_4$**, **Sub$_5$**, and **Sub$_6$** exhibit storage energies of 143.2, 166.7, and 158.4 kJ mol^{-1} and the corresponding TBR barriers are 120.9, 121.7, and 129.6 kJ mol^{-1}, respectively, underscoring their strong energy storage and retention capabilities. A pronounced red-shift in excitation wavelength and an increase in the molar absorption coefficient are observed upon solvation, while spectral overlap is minimized, favoring features for efficient photoisomerization.

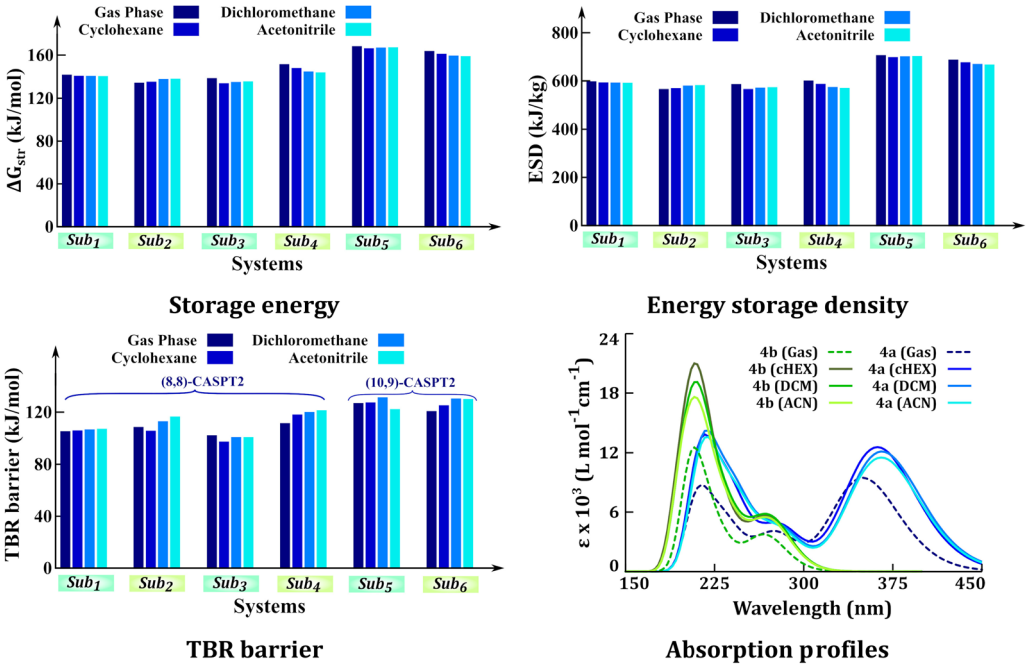

Fig. 4 Effect of solvation on the thermochemical properties and absorption profile of the studied functionalized BBD-based photoswitches.

Overall, highly polar solvents play a crucial role in enhancing energy storage duration and optimizing the absorption characteristics without compromising the intrinsic energy storage performance of these photoswitches.

3.4. Electronic structure analysis

The thermal reversion of the metastable photoproduct to the parent diene follows a highly asynchronous yet concerted mechanism for dissociation of σ-bonds, wherein α-bond dissociation precedes that of the β-bond.[21,55,56] As a result, the α-bond distances in the TS structure are significantly longer than the β-bond distances, as illustrated in Fig. 5a. This asynchronous cleavage introduces biradicaloid character in the TS. As these structural and electronic parameters are critical in governing the photoswitching behavior, we examined the two dissociating σ-bond lengths and the active space orbital occupancies in the TS.

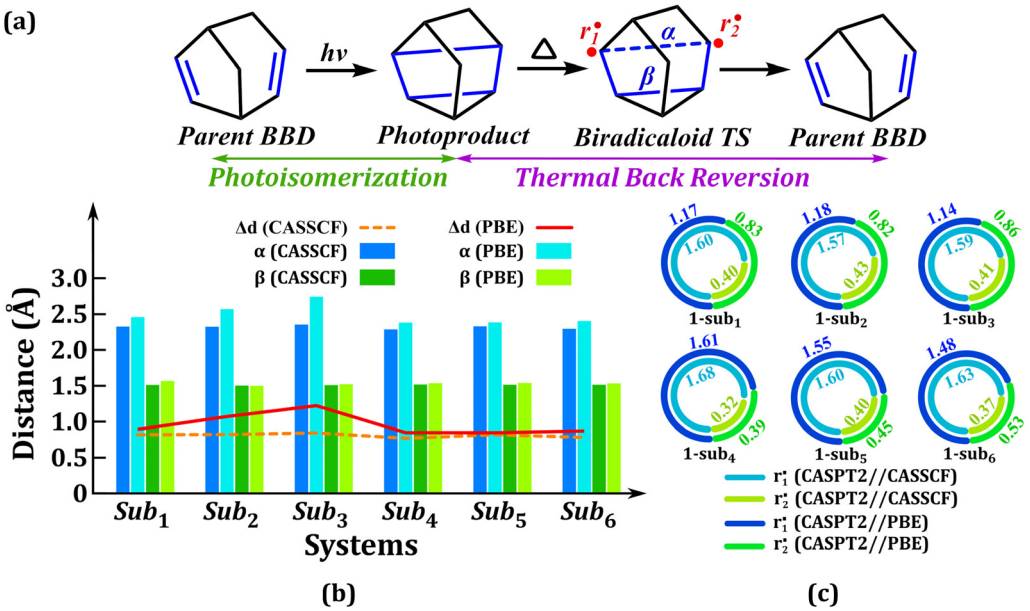

Fig. 5 (a) Schematic representation of the mechanism for the asynchronous thermal back reversion in BBD-based photoswitches, (b) the α- and β-bond distances, along with their differences ($\Delta d = \alpha - \beta$) computed using the two computational approaches, and (c) active space orbital occupancies for the singlet biradicaloid as determined by the two methods.

The α- and β-bond distances, along with their differences (Δd = α–β), are shown in Fig. 5 and numerical values are summarized in Table S5 (S V of SI). The CASSCF method predicts α-bond lengths in the range of 2.27–2.34 Å, which are 0.05–0.39 Å shorter than those estimated using the PBE method (2.37–2.55 Å). In contrast, the β-bond distances from CASSCF (1.49–1.50 Å) show only minor deviations (maximum 0.06 Å) relative to the PBE-calculated values (1.48–1.55 Å). The Δd values obtained from PBE range from 0.85 to 1.22 Å, effectively capturing the high asynchronicity of the reaction. These results are in agreement with our recent reports where similar Δd values were observed for the various unsubstituted BBD-based photoswitches.[45] The CASSCF-derived Δd values are smaller (0.77 to 0.85 Å), suggesting less asynchronicity compared to PBE.

The terms $r_1^\bullet$ and $r_2^\bullet$ refer to the occupation numbers (ONs) of the two orbitals involved in the biradical formation. These orbitals arise due to the cleavage of the α-bond in the highly asynchronous dissociation mechanism. These ON values were obtained from the active space orbitals derived from single-point CASPT2/6-311++G** calculations performed on the TS geometries. The active space orbitals employed in the CASPT2 calculations are illustrated using the TS geometries of **Sub$_4$** and **Sub$_5$** in Fig. S3 (S V of SI). A system is characterized as a biradical when both ONs are close to 1.0, indicating the presence of two unpaired electrons in separate orbitals. When the ONs of these orbitals deviate from 1.0 and lie between 0 and 2, the system is better described as a biradicaloid, implying partial biradical characteristics with a multiconfigurational nature. The occupancies of the biradicaloid $r_1^\bullet$ and $r_2^\bullet$ are schematically illustrated in Fig. 5c, and the values are tabulated in Table S5 (S V of SI).

The orbital occupancies in the TS geometries of **Sub$_1$** to **Sub$_3$** predicted using CASPT2//PBE show nearly equivalent electronic distribution in $r_1^\bullet$ (1.14–1.18) and $r_2^\bullet$ (0.82–0.86). Thus, the active space orbitals of the TS geometries obtained using PBE approximately uphold the $r_1^\bullet = r_2^\bullet = \sim 1$ relations, indicating that they exhibit a pronounced biradicaloid character. In contrast, CASPT2//CASSCF predicts an imbalanced electron distribution in $r_1^\bullet$ (1.57–1.68) and $r_2^\bullet$ (0.32–0.43) in the TS for **Sub$_1$** to **Sub$_6$**. Such an uneven orbital occupation number has been previously reported and is known to exhibit a biradicaloid character.[64] Analogous to the CASPT2//CASSCF method, CASPT2//PBE also predicts a larger difference in the occupancies of $r_1^\bullet$ (1.48–1.61) and $r_2^\bullet$ (0.39–0.52) in the TS for **Sub$_4$** to **Sub$_6$**. Thus, both the level of theories predicts **Sub$_4$** to **Sub$_6$** to exhibit a reduced biradicaloid character compared to **Sub$_1$** to **Sub$_3$**.

In the asynchronous TS of thermal reversion, the extent of α-bond dissociation governs the biradicaloid character. The significant elongation of the α-bond (larger Δd) leads to nearly equal orbital ONs $\left(r_1^\bullet \approx r_2^\bullet \approx 1\right)$, reflecting balanced electron distribution. However, in cases where α-bond dissociation is relatively less pronounced (smaller Δd), the electron density remains localized, resulting in imbalanced occupation numbers $\left(r_1^\bullet > r_2^\bullet\right)$. This behavior highlights a direct correlation between the geometry of the TS and its electronic structure. The correlation plot between the degree of asynchronicity in the TS and the difference in ONs of the singlet biradicaloid is depicted in Fig. S4 (S V of SI).

It is worth mentioning that the degree of asynchronicity and the orbital occupation pattern exhibit correlations with the TBR barrier of the metastable photoproduct (Fig. S4). Systems with highly asynchronous TSs and pronounced biradicaloid character (more symmetric occupation) tend to be more stable and exhibit lower TBR barriers. On the contrary, systems with fewer asynchronous TSs and asymmetric orbital occupation are less effective in stabilizing the TS, thereby requiring higher TBR barriers. Therefore, the TBR barrier of **Sub$_4$** to **Sub$_6$** are remarkably high among all the studied functionalized BBD-based photoswitches. These findings suggest that an effective photoswitch design should favor increased biradicaloid asymmetry to achieve longer energy storage durations. The TS geometries optimized using CASSCF less effectively capture the high asynchronicity of the reaction and predict reduced biradicaloid nature than PBE, as verified by CASPT2 single-point calculations. Consequently, the TBR barriers predicted *via* CASPT2 single-point calculations on CASSCF/6-311++G** geometries are significantly higher than those obtained from the PBE/6-311++G** optimized structures.

3.5. Molecular designing strategy for synergistic control of electron behaviour

As expected, the nature and position of the substituents have a substantial impact on the thermochemical properties of the photoswitch. Based on the exhibited properties, design inferences have been drawn that will aid in improving the photoswitching properties in the future. While similar substituents are introduced, at the two distinct unsaturated bridges of the BBD, the energy storage capacity of **Sub$_1$** is 7.52 kJ mol^{-1} and **Sub$_3$** is 4.25 kJ mol^{-1} greater than **Sub$_2$** in the gas phase (DLPNO-CCSD(T)). This signifies that systems functionalized on a non-elongated bridge (**Sub$_1$** and **Sub$_3$**) have a relatively higher energy storage capacity than those functionalized on an elongated bridge (**Sub$_2$**). The functionalization of BBD with a methoxy phenyl group as an electron donor (**Sub$_1$**) provide higher energy storage capacity and storage time than the methyl aniline group in **Sub$_3$**. The larger electron releasing tendency of methyl aniline may be attributed to the comparatively easier thermal ring opening of the photoproduct of **Sub$_3$**. Moreover, BBD systems functionalized at an elongated unsaturated bridge, including that elongated with –NH– units (**Sub$_2$** and **Sub$_5$**), are found to have a better TBR barrier.

It is worth mentioning that substituents in **Sub$_4$** participate in intramolecular hydrogen-bonding interactions, wherein the hydrogen atom of the methyl aniline group interacts with lp on O, thereby stabilizing the photoproduct and TS structure. The existence of H-bonding interaction in the TS of **Sub$_4$** is evidenced from the IRI analysis (Fig. 6). As a result, additional energy is required for the ring-opening of the [2+2]-cycloadduct, raising the thermal reversion barrier by 9.32 kJ mol^{-1} relative to **Sub$_3$**. Close analysis reveals that the H-bonding interactions restrict the large separation of the α-bond in the TS structure

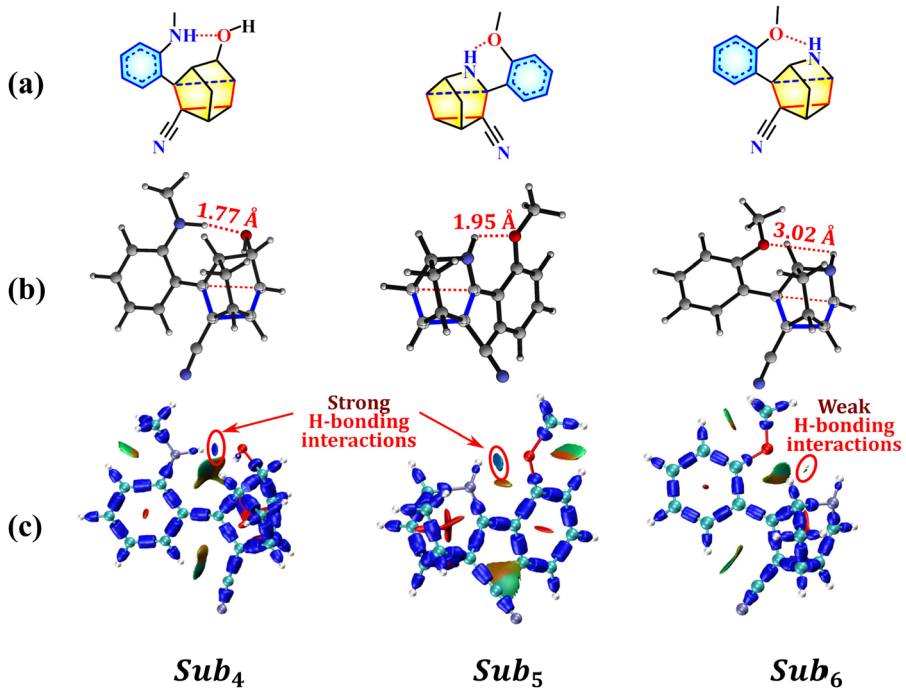

Fig. 6 (a) Molecular structure of the TS involved in thermal reversion, (b) optimized TS geometries, and (c) IRI plot of the TS.

during the thermal back reversion of the metastable photoproduct in **Sub$_4$**. Consequently, the degree of asynchronicity and the biradicaloid character are reduced in **Sub$_4$** comparative to the **Sub$_3$**. In essence, the hydrogen bond acts as a tether between the dissociating bridges of the photoproduct, necessitating extra energy for the thermal back-conversion. The orbital occupancies $(r_1^\bullet, r_2^\bullet)$ in the TS for **Sub$_5$** (1.55, 0.45) and **Sub$_6$** (1.48, 0.53) obtained even with PBE indicate inequivalent electron distribution between the two radicals, likely due to electron density interference from the lp of conjugated N. Consequently, BBDs with –NH– elongated bridges show significantly higher TBR barriers than those extended with –CH_2– linkers. This finding highlights the potential of rational substituent designs to introduce stabilizing non-covalent interactions that enhance the thermochemical performance of photoswitches for solar thermal energy storage.

4. Conclusion

The functionalized BBD-based photochromic systems with elongated unsaturated bridges exhibit remarkable energy storage capacities (133.6–167.7 kJ mol^{-1} at the DLPNO-CCSD(T) level), establishing their strong potential for MOST applications. The strategic incorporation of electron-donating and -withdrawing substituents enables significant bathochromic shifts in absorption, although with a trade-off in thermal stability. It is notable that synergistic non-covalent interactions and push–pull electronic effects enable substantial red-shifts in absorption wavelengths without compromising thermochemical performance. Notably, the participation of the lone pair on the donor heteroatom in intramolecular hydrogen bonding slightly reduces the red-shift, suggesting that such interactions should be avoided to preserve the full push–pull effect and maximize solar absorption efficiency. The asynchronicity in the TS structure and the occupancies of the singlet biradicaloid significantly affect the TBR barrier of the photoswitch. The H-bonding interactions restrict the large separation of the α-bond, and consequently, the degree of asynchronicity and the biradicaloid character in the TS structure, thereby elevating the TBR barrier. Highly polar solvents play a crucial role in enhancing energy storage duration and optimizing absorption characteristics without compromising the intrinsic energy storage performance. The **Sub$_4$** system exhibits a storage energy (density) of 150.9 kJ mol^{-1} (546.7 kJ kg^{-1}), TBR barrier (half-life) of 111.2 kJ mol^{-1} (1.34 days) and λ_{onset} (λ) of 460 nm (350 nm), making it suitable for day-night photoswitching cycles in window coating applications. The **Sub$_5$** exhibits a storage energy of 167.28 kJ mol^{-1}, TBR barrier of 126.4 kJ mol^{-1}, allowing it to retain the stored energy for up to 51.47 years, thus demonstrating strong potential for long-term energy storage applications.

Author contributions

AAS: conceptualization, data curation, formal analysis, investigation, methodology, validation, visualization, writing – original draft, writing – review & editing; RKK: formal analysis, investigation, visualization, writing – review & editing; SS: data curation, formal analysis, visualization, writing – original draft, and RP:

funding acquisition, project administration, software, resources, supervision, validation, writing – review & editing.

Conflicts of interest

The authors declare that there are no conflicts of interest.

Data availability

The data that support the findings of this work are provided in the SI, and the Cartesian coordinates of the optimized geometry point structures are given in a single Cartesian.xyz file.

Optimized geometries of BBD, photoproducts, and TS structure, thermochemical properties calculated using M06-2X/6-311++G**, DLPNO-CCSD(T)/Def2-TZVP and CASPT2/6-311++G** level in gas phase and in presence of different polarity solvents, absorption properties of the functionalized dienes and photoproducts, the two dissociating bond distances (α and β) and active space orbital and occupancies ($r_1^\bullet$ and $r_2^\bullet$) in the TS structure, Correlation plots between the difference in distances, occupancies in TS and the TBR barrier. The Cartesian coordinates of the optimized geometries of the photoisomers are provided in the file Cartesian.xyz. See DOI: **https://doi.org/10.1039/d5cp01525a**

Acknowledgements

We are sincerely thankful to the DST-SERB (EEQ/2023/000424, ECR/2018/002346 and EEQ/2019/000656) for providing financial support for this work. We are grateful to the Director, National Institute of Technology Warangal (NITW), India, for providing us the platform to perform this work. AAS and RKK wish to thank the Ministry of Education (MoE), India, for the SRF.

References

1 H. Pontzer and A. McGrosky, Balancing growth, reproduction, maintenance, and activity in evolved energy economies, *Curr. Biol.*, 2022, **32**, R709–R719.
2 N. S. Lewis and D. G. Nocera, Powering the planet: Chemical challenges in solar energy utilization, *Proc. Natl. Acad. Sci. U. S. A.*, 2006, **103**, 15729–15735.
3 M. Grätzel, Powering the planet, *Nature*, 2000, **403**, 363.
4 M. Asif and T. Muneer, Energy supply, its demand and security issues for developed and emerging economies, *Renewable Sustainable Energy Rev.*, 2007, **11**, 1388–1413.
5 Q. Wang and K. Domen, Particulate Photocatalysts for Light-Driven Water Splitting: Mechanisms, Challenges, and Design Strategies, *Chem. Rev.*, 2020, **120**, 919–985.
6 P. Ganji, R. K. Chowdari and B. Likozar, Photocatalytic Reduction of Carbon Dioxide to Methanol: Carbonaceous Materials, Kinetics, Industrial Feasibility, and Future Directions, *Energy Fuels*, 2023, **37**, 7577–7602.
7 A. K. Jena, A. Kulkarni and T. Miyasaka, Halide Perovskite Photovoltaics: Background, Status, and Future Prospects, *Chem. Rev.*, 2019, **119**, 3036–3103.
8 B. S. Richards, D. Hudry, D. Busko, A. Turshatov and I. A. Howard, Photon Upconversion for Photovoltaics and Photocatalysis: A Critical Review, *Chem. Rev.*, 2021, **121**, 9165–9195.
9 E. Collini, Light-Harvesting: The Never-Ending Lesson of Nature, *ACS Cent. Sci.*, 2022, **8**, 306–308.
10 G. D. Scholes, G. R. Fleming, A. Olaya-Castro and R. van Grondelle, Lessons from nature about solar light harvesting, *Nat. Chem.*, 2011, **3**, 763–774.
11 D. G. Nocera, The Artificial Leaf, *Acc. Chem. Res.*, 2012, **45**, 767–776.
12 J. Usuba and G. G. D. Han, Photoswitch designs for molecular solar thermal energy storage, *Trends Chem.*, 2023, **5**, 577–580.
13 Z. Wang, P. Erhart, T. Li, Z.-Y. Zhang, D. Sampedro, Z. Hu, H. A. Wegner, O. Brummel, J. Libuda, M. B. Nielsen and K. Moth-Poulsen, Storing energy with molecular photoisomers, *Joule*, 2021, **5**, 3116–3136.
14 T. J. Kucharski, Y. Tian, S. Akbulatov and R. Boulatov, Chemical solutions for the closed-cycle storage of solar energy, *Energy Environ. Sci.*, 2011, **4**, 4449–4472.
15 Q. Qiu, S. Yang, M. A. Gerkman, H. Fu, I. Aprahamian and G. G. D. Han, Photon Energy Storage in Strained Cyclic Hydrazones: Emerging Molecular Solar Thermal Energy Storage Compounds, *J. Am. Chem. Soc.*, 2022, **144**, 12627–12631.
16 A. Lennartson, A. Roffey and K. Moth-Poulsen, Designing photoswitches for molecular solar thermal energy storage, *Tetrahedron Lett.*, 2015, **56**, 1457–1465.
17 A. A. Sangolkar, A. Shahi, R. K. Kadiyam and R. Pawar, Origin of a Kinetically Selective Route for Thermoreversible Valence Tautomerism-Based Photoswitching in O-Heterocycles Containing Conjugated Dienes, *J. Org. Chem.*, 2024, **89**, 15497–15512.
18 A. A. Sangolkar, R. K. Kadiyam and R. Pawar, Resolving the Ambiguity of Thermal Reversion in a Nonconjugated Monocyclic Diene-Based Photoswitch for Rechargeable Solar Thermal Batteries, *J. Phys. Chem. A*, 2025, **129**(6), 1529–1541.
19 A. A. Sangolkar, R. K. Kadiyam and R. Pawar, An unprecedented double photoexcitation mechanism for photoswitching in conjugated-dienes to trigger physiological processes for photopharmacology, *Org. Biomol. Chem.*, 2025, **23**, 1909–1922.
20 J. Orrego-Hernández, A. Dreos and K. Moth-Poulsen, Engineering of Norbornadiene/Quadricyclane Photoswitches for Molecular Solar Thermal Energy Storage Applications, *Acc. Chem. Res.*, 2020, **53**, 1478–1487.
21 K. Jorner, A. Dreos, R. Emanuelsson, O. E. Bakouri, I. F. Galván, K. Börjesson, F. Feixas, R. Lindh, B. Zietz, K. Moth-Poulsen and H. Ottosson, Unraveling factors leading to efficient norbornadiene–quadricyclane molecular solar-thermal energy storage systems, *J. Mater. Chem. A*, 2017, **5**, 12369–12378.
22 M. Mansø, A. U. Petersen, Z. Wang, P. Erhart, M. B. Nielsen and K. Moth-Poulsen, Molecular solar thermal energy

storage in photoswitch oligomers increases energy densities and storage times, *Nat. Commun.*, 2018, **9**, 1945.
23 C.-L. Sun, C. Wang and R. Boulatov, Applications of Photoswitches in the Storage of Solar Energy, *ChemPhotoChem*, 2019, **3**, 268–283.
24 Z. Wang, Z. Wu, Z. Hu, J. Orrego-Hernández, E. Mu, Z.-Y. Zhang, M. Jevric, Y. Liu, X. Fu, F. Wang, T. Li and K. Moth-Poulsen, Chip-scale solar thermal electrical power generation, *Cell Rep. Phys. Sci.*, 2022, **3**, 100789.
25 Z. Wang, H. Moïse, M. Cacciarini, M. B. Nielsen, M. Morikawa, N. Kimizuka and K. Moth-Poulsen, Liquid-Based Multijunction Molecular Solar Thermal Energy Collection Device, *Adv. Sci.*, 2021, **8**, 2103060.
26 F. Waidhas, M. Jevric, M. Bosch, T. Yang, E. Franz, Z. Liu, J. Bachmann, K. Moth-Poulsen, O. Brummel and J. Libuda, Electrochemically controlled energy release from a norbornadiene-based solar thermal fuel: increasing the reversibility to 99.8% using HOPG as the electrode material, *J. Mater. Chem. A*, 2020, **8**, 15658–15664.
27 Z. Refaa, A. Hofmann, M. F. Castro, J. O. Hernandez, Z. Wang, H. Hölzel, J. W. Andreasen, K. Moth-Poulsen and A. S. Kalagasidis, Thermo-optical performance of molecular solar thermal energy storage films, *Appl. Energy*, 2022, **310**, 118541.
28 A. U. Petersen, A. I. Hofmann, M. Fillols, M. Mansø, M. Jevric, Z. Wang, C. J. Sumby, C. Müller and K. Moth-Poulsen, Solar Energy Storage by Molecular Norbornadiene–Quadricyclane Photoswitches: Polymer Film Devices, *Adv. Sci.*, 2019, **6**, 1900367.
29 J. Mony, C. Climent, A. U. Petersen, K. Moth-Poulsen, J. Feist and K. Börjesson, Photoisomerization Efficiency of a Solar Thermal Fuel in the Strong Coupling Regime, *Adv. Funct. Mater.*, 2021, **31**, 2010737.
30 V. Gray, A. Lennartson, P. Ratanalert, K. Börjesson and K. Moth-Poulsen, Diaryl-substituted norbornadienes with red-shifted absorption for molecular solar thermal energy storage, *Chem. Commun.*, 2014, **50**, 5330–5332.
31 K. Börjesson, A. Lennartson and K. Moth-Poulsen, Efficiency Limit of Molecular Solar Thermal Energy Collecting Devices, *ACS Sustainable Chem. Eng.*, 2013, **1**, 585–590.
32 W. Sun, Z. Shangguan, X. Zhang, T. Dang, Z.-Y. Zhang and T. Li, Solar Efficiency of Azo-Photoswitches for Energy Conversion: A Comprehensive Assessment, *ChemSusChem*, 2023, **16**, e202300582.
33 Q. Qiu, Y. Shi and G. G. D. Han, Solar energy conversion and storage by photoswitchable organic materials in solution, liquid, solid, and changing phases, *J. Mater. Chem. C*, 2021, **9**, 11444–11463.
34 Z. Wang, H. Hölzel and K. Moth-Poulsen, Status and challenges for molecular solar thermal energy storage system based devices, *Chem. Soc. Rev.*, 2022, **51**, 7313–7326.
35 X. Xu and G. Wang, Molecular Solar Thermal Systems towards Phase Change and Visible Light Photon Energy Storage, *Small*, 2022, **18**, 2107473.
36 A. Giménez-Gómez, L. Magson, C. Merino-Robledillo, S. Hernáez-Troya, N. Sanosa, D. Sampedro and I. Funes-Ardoiz, State-of-the-art and challenges towards a Molecular Solar Thermal (MOST) energy storage device, *React. Chem. Eng.*, 2024, **9**, 1629–1640.
37 R. J. Salthouse and K. Moth-Poulsen, Multichromophoric photoswitches for solar energy storage: from azobenzene to norbornadiene, and MOST things in between, *J. Mater. Chem. A*, 2024, **12**, 3180–3208.
38 M. Quant, A. E. Hillers-Bendtsen, S. Ghasemi, M. Erdelyi, Z. Wang, L. M. Muhammad, N. Kann, K. V. Mikkelsen and K. Moth-Poulsen, Synthesis, characterization and computational evaluation of bicyclooctadienes towards molecular solar thermal energy storage, *Chem. Sci.*, 2022, **13**, 834–841.
39 A. E. Hillers-Bendtsen, M. Quant, K. Moth-Poulsen and K. V. Mikkelsen, Investigation of the Structural and Thermochemical Properties of [2.2.2]-Bicyclooctadiene Photoswitches, *J. Phys. Chem. A*, 2021, **125**, 10330–10339.
40 A. E. Hillers-Bendtsen, J. L. Elholm, O. B. Obel, H. Hölzel, K. Moth-Poulsen and K. V. Mikkelsen, Searching the Chemical Space of Bicyclic Dienes for Molecular Solar Thermal Energy Storage Candidates, *Angew. Chem., Int. Ed.*, 2023, **62**, e202309543.
41 A. A. Sangolkar, R. K. Kadiyam and R. Pawar, Novel route to enhance the thermo-optical performance of bicyclic diene photoswitches for solar thermal batteries, *Beilstein J. Org. Chem.*, 2024, **20**, 1053–1068.
42 A. A. Sangolkar, M. Faizan, K. R. Krishna and R. Pawar, Azabicyclooctadiene/tetracyclooctane couples as promising photoswitches for molecular solar thermal energy storage applications, *Mol. Syst. Des. Eng.*, 2023, **8**, 853–865.
43 A. E. Hillers-Bendtsen, Y. Zhou and K. V. Mikkelsen, Investigation of Solvent Effects on the Molecular Energy Storage and Optical Properties of Bicyclooctadiene/Tetracyclooctane Photoswitches, *J. Phys. Chem. A*, 2024, **128**, 41–50.
44 A. A. Sangolkar, R. K. Kadiyam and R. Pawar, Azabicyclodiene based photoswitches for molecular solar thermal energy storage, *Energy Adv.*, 2024, **3**, 287–298.
45 A. A. Sangolkar, R. K. Kadiyam and R. Pawar, Strain Engineered Bridged Bicyclic Diene Photoswitches in the Race of Next-Generation Molecular Solar Thermal Energy Storage, *ChemPhotoChem*, 2024, **8**, e202400089.
46 A. E. Hillers-Bendtsen, P. G. Iuel Lunøe Dünweber, L. H. Olsen and K. V. Mikkelsen, Prospects of Improving Molecular Solar Energy Storage of the Norbornadiene/Quadricyclane System through Bridgehead Modifications, *J. Phys. Chem. A*, 2022, **126**, 2670–2676.
47 J. Calbo, C. E. Weston, A. J. P. White, H. S. Rzepa, J. Contreras-García and M. J. Fuchter, Tuning Azoheteroarene Photoswitch Performance through Heteroaryl Design, *J. Am. Chem. Soc.*, 2017, **139**, 1261–1274.
48 T. Dang, Z.-Y. Zhang and T. Li, Visible-Light-Activated Heteroaryl Azoswitches: Toward a More Colorful Future, *J. Am. Chem. Soc.*, 2024, **146**, 19609–19620.
49 Y. Zhao and D. G. Truhlar, The M06 suite of density functionals for main group thermochemistry, thermochemical kinetics, noncovalent interactions, excited states, and transition elements: two new functionals and systematic

testing of four M06-class functionals and 12 other functionals, *Theor. Chem. Acc.*, 2008, **120**, 215–241.
50 N. Ree and K. V. Mikkelsen, Benchmark study on the optical and thermochemical properties of the norbornadiene-quadricyclane photoswitch, *Chem. Phys. Lett.*, 2021, **779**, 138665.
51 Y. Guo, C. Riplinger, U. Becker, D. G. Liakos, Y. Minenkov, L. Cavallo and F. Neese, Communication: An improved linear scaling perturbative triples correction for the domain based local pair-natural orbital based singles and doubles coupled cluster method [DLPNO-CCSD(T)], *J. Chem. Phys.*, 2018, **148**, 011101.
52 R. K. Kadiyam, A. A. Sangolkar, M. Faizan and R. Pawar, Bispericyclic Ambimodal Dimerization of Pentafulvene: The Origin of Asynchronicity and Kinetic Selectivity of the Endo Transition State, *J. Org. Chem.*, 2024, **89**, 6813–6825.
53 R. K. Kadiyam, A. A. Sangolkar and R. Pawar, Symmetric and Unsymmetric Bifurcating Surfaces of Ambimodal Reactions: Origin of Electronic Behavior in Post-Transition State Bifurcation, *J. Org. Chem.*, 2025, **90**(29), 10170–10182.
54 R. Hoffmann and R. B. Woodward, Selection Rules for Concerted Cycloaddition Reactions, *J. Am. Chem. Soc.*, 1965, **87**, 2046–2048.
55 M. J. Kuisma, A. M. Lundin, K. Moth-Poulsen, P. Hyldgaard and P. Erhart, Comparative Ab-Initio Study of Substituted Norbornadiene-Quadricyclane Compounds for Solar Thermal Storage, *J. Phys. Chem. C*, 2016, **120**, 3635–3645.
56 M. Mansø, A. U. Petersen, K. Moth-Poulsen and M. B. Nielsen, Establishing linear-free-energy relationships for the quadricyclane-to-norbornadiene reaction, *Org. Biomol. Chem.*, 2020, **18**, 2113–2119.
57 K. Andersson, P. Aake. Malmqvist, B. O. Roos, A. J. Sadlej and K. Wolinski, Second-order perturbation theory with a CASSCF reference function, *J. Phys. Chem.*, 1990, **94**, 5483–5488.
58 P. E. M. Siegbahn, J. Almlöf, A. Heiberg and B. O. Roos, The complete active space SCF (CASSCF) method in a Newton–Raphson formulation with application to the HNO molecule, *J. Chem. Phys.*, 1981, **74**, 2384–2396.
59 J. Paier, R. Hirschl, M. Marsman and G. Kresse, The Perdew–Burke–Ernzerhof exchange-correlation functional applied to the G2-1 test set using a plane-wave basis set, *J. Chem. Phys.*, 2005, **122**, 234102.
60 F. Neese, Software update: the ORCA program system, version 4.0, *Wiley Interdiscip. Rev.: Comput. Mol. Sci.*, 2018, **8**, e1327.
61 M. J. Frisch, G. W. Trucks, H. B. Schlegel, G. E. Scuseria, M. A. Robb, J. R. Cheeseman, G. Scalmani, V. Barone, G. A. Petersson, H. Nakatsuji, X. Li, M. Caricato, A. V. Marenich, J. Bloino, B. G. Janesko, R. Gomperts, B. Mennucci, H. P. Hratchian, J. V. Ortiz, A. F. Izmaylov, J. L. Sonnenberg, D. Williams-Young, F. Ding, F. Lipparini, F. Egidi, J. Goings, B. Peng, A. Petrone, T. Henderson, D. Ranasinghe, V. G. Zakrzewski, J. Gao, N. Rega, G. Zheng, W. Liang, M. Hada, M. Ehara, K. Toyota, R. Fukuda, J. Hasegawa, M. Ishida, T. Nakajima, Y. Honda, O. Kitao, H. Nakai, T. Vreven, K. Throssell, J. A. Montgomery Jr., J. E. Peralta, F. Ogliaro, M. J. Bearpark, J. J. Heyd, E. N. Brothers, K. N. Kudin, V. N. Staroverov, T. A. Keith, R. Kobayashi, J. Normand, K. Raghavachari, A. P. Rendell, J. C. Burant, S. S. Iyengar, J. Tomasi, M. Cossi, J. M. Millam, M. Klene, C. Adamo, R. Cammi, J. W. Ochterski, R. L. Martin, K. Morokuma, O. Farkas, J. B. Foresman and D. J. Fox, *Gaussian 16 Rev. C.01*, 2016.
62 T. Lu and F. Chen, Multiwfn: A multifunctional wavefunction analyzer, *J. Comput. Chem.*, 2012, **33**, 580–592.
63 T. Lu and Q. Chen, Interaction Region Indicator: A Simple Real Space Function Clearly Revealing Both Chemical Bonds and Weak Interactions**, *Chemistry—Methods*, 2021, **1**(5), 231–239.
64 D. Doehnert and J. Koutecky, Occupation numbers of natural orbitals as a criterion for biradical character. Different kinds of biradicals, *J. Am. Chem. Soc.*, 1980, **102**, 1789–1796.